PCCP

ROYAL SOCIETY OF CHEMISTRY

PAPER

View Article Online
View Journal

Cite this: DOI: 10.1039/d1cp04836h

Elastic moduli of normal and cancer cell membranes revealed by molecular dynamics simulations†

Hoang Linh Nguyen, [a] Viet Hoang Man,[b] Mai Suan Li, [ac] Philippe Derreumaux,[d] Junmei Wang [b] and Phuong H. Nguyen *[de]

Received 22nd October 2021,
Accepted 15th February 2022

DOI: 10.1039/d1cp04836h

rsc.li/pccp

Recent studies indicate that there are mechanical differences between normal cells and cancer cells. Because the cell membrane takes part in a variety of vital processes, we test the hypothesis of whether or not two fundamental alterations in the cell membrane, *i.e.*, the overexpression of phosphatidylserine lipids in the outer leaflet and a reduction in cholesterol concentration, could cause the softening in cancer cells. Adopting ten models of normal and cancer cell membranes, we carry out 1 μs all-atom molecular dynamics simulations to compare the structural properties and elasticity properties of two membrane types. We find that the overexpression of the phosphatidylserine lipids in the outer leaflet does not significantly alter the area per lipid, the membrane thickness, the lipid order parameters and the elasticity moduli of the cancer membranes. However, a reduction in the cholesterol concentration leads to clear changes in those quantities, especially decreases in the bending, tilt and twist moduli. This implies that the reduction of cholesterol concentration in the cancer membranes could contribute to the softening of cancer cells.

1 Introduction

Cancer is a serious problem affecting the health of all human societies. Basically, it is the uncontrolled growth of abnormal cells in the body. These cells have the ability to spread, leading to the appearance of tumors in organs located far away from the primary tumor site.[1] During the spread, cancer cells must pass through many obstacles such as small gaps in basement membranes, blood vessels and crowded environments in the body. Therefore, it has been suggested that cancer cells must be soft and deformable to perform such a task.[2] Indeed, a growing number of experimental techniques are being used to study the mechanical properties of cancer cell lines or primary cells from biopsies,[3–5] and the results clearly indicate that cancer cells from a large number of different organs are softer than their normal counterparts. This may be due to alterations in the extracellular environment, as well as in the intracellular elements such as the cell microenvironment, the cytoskeleton, the nucleus, the intracellular compartments, the signalling proteins, the active forces, the internal membrane and the plasma membrane.[2] Understanding which cell elements contribute to the softness of cancer cells could be very important for the development of efficient diagnosis and treatment methods. In this work, we only focus on the cell membrane element, and try to understand if fundamental alterations in the membrane properties cause the cancer cells to be softer than the normal counterparts.

Normal cell membranes have a highly asymmetric lipid composition.[6] That is, the extracellular leaflet is mainly composed of phosphatitylcholine (PC) and sphingo lipids, and the intracellular leaflet is mostly composed of phosphatidylethanolamine (PE) and phosphatidylserine (PS) lipids. Is is known that the concentration of the negatively charged PS lipids is increased by 5–9 times in the outer leaflet when normal membranes are transformed to cancer membranes, and this is usually considered as a biological cue that is related to the apoptotic pathway.[7,8] As a consequence, cancer membranes have a less negative membrane potential than those of normal membranes.[9–11] Another alteration in cancer cells is a reduction in the cholesterol concentration in their membranes,[12] which

[a] *Institute for Computational Science and Technology, SBI Building, Quang Trung Software City, Tan Chanh Hiep Ward, District 12, Ho Chi Minh City, Vietnam*
[b] *Department of Pharmaceutical Sciences, School of Pharmacy, University of Pittsburgh, Pittsburgh, PA 15213, USA*
[c] *Institute of Physics, Polish Academy of Sciences, Al. Lotnikow 32/46, 02-668 Warsaw, Poland*
[d] *CNRS, Université de Paris, UPR9080, Laboratoire de Biochimie Théorique, Paris, France*
[e] *Institut de Biologie Physico-Chimique, Fondation Edmond de Rothschild, PSL Research University, Paris, France. E-mail: nguyen@ibpc.fr*

† Electronic supplementary information (ESI) available. See DOI: 10.1039/d1cp04836h

results in decreases of the order of lipid hydrocarbon chains and membrane thickness, and an increase in the surface area of lipids.[13–17] However, effects due to the reduction of cholesterol concentration and the overexpression of negatively charged PS lipids in the outer leaflet on the elastic properties of cancer membranes have not yet been studied to the best of our knowledge.

Molecular dynamics (MD) simulations have provided valuable information on the structural and dynamic properties of lipid bilayers. In the early days, MD simulations of membrane models considered only single-component lipid bilayers;[18–20] later simulations have incorporated more than one lipid component as well as cholesterol.[21] However, many of these multiple-component lipid simulations were performed on symmetric bilayers containing the same lipid mole fractions of both leaflets. Recently, several MD simulations on asymmetric bilayers have also been reported.[6,22,23] Despite many MD simulations of lipid membranes having been carried out, there is little work on the modelling of the membranes of cancer cells. Only a few cancer membrane computational models have been developed recently.[24–26]

The main aim of this work is to employ MD simulations to theoretically study the effects of the two mentioned alterations, *i.e.*, the overexpression of the PS lipid concentration in the extracellular leaflet, and the reduction of the cholesterol concentration on the elasticity properties of normal and cancer cell membranes. This may provide some insight into the differences in the mechanical properties of the two cell types. From a theoretical perspective, many studies have used the traditional Canham–Helfrich model of membrane fluctuations to calculate the bending modulus K_c.[27,28] Later, May *et al.* extended this model to include molecular tilting.[29] This extension is widely considered to be important for understanding membrane fusion.[30] Recently, Watson *et al.* have provided a theoretical model to include three elastic moduli, *i.e.*, bending, tilt and twist, which can be extracted from MD simulations data in Fourier space.[31–34] Very recently, Khelashvili *et al.* have developed a method that enables calculation of the bending modulus K_c from local fluctuations on the molecular scale in real space.[35–38] On the experimental side, for many years, experiments have used the Canham–Helfrich model to analyse diffuse X-ray scattering in order to obtain values for K_c.[39] Unfortunately, the results for K_c of chemically identical membranes, obtained from different experiments, are usually substantially different,[40] even for single-component lipid membranes. Furthermore, there are nearly no experimental data for multiple-component lipid membranes.

In this work, we carry out all-atom MD simulations of five normal membrane models and five cancer membrane models taken from previous studies.[24–26] All these models have the same lipid compositions, *i.e.*, the same number of total lipids, but differ in the lipid mole fractions of the outer and inner leaflets, and in the cholesterol concentration. From our simulation data, various structural quantities are characterized, and the bilayer bending, tilt and twist moduli are calculated, which allows us to compare the structural and elasticity properties of normal and cancer cell membranes.

2 Methodology

2.1 Membrane models

First, we constructed four normal membrane models based on the models of previous studies. Rivel *et al.*[24] constructed models using the lipid contents of the mammalian erythrocyte membrane obtained from two different experiments.[41,42] Based on their models, and using the same mole fractions of lipids and cholesterol, we construct two normal membrane models, named M1 and M2. Our third normal membrane model, named M3, is constructed using the lipid mole fractions of the model of Klahn *et al.*,[25] which was built using other experimental data of erythrocyte cells.[43] The fourth normal membrane model (M4) is built using the mole fractions of lipids of the model of Ingolfsson *et al.*, which was constructed using the general properties of cell membranes found within the brain.[26] Each model contains four lipid types: 1,2-dioleoyl-*sn-glycero*-3-phosphocholine (DOPC), sphingomyelin (SM) lipids, dioleoyl-*sn-glycero*-3-phosphoethanolamine (DOPE) and 1,2-dioleoyl-*sn-glycero*-3-phospho-L-serine (DOPS) lipids. Following the work of Rivel *et al.*, we add ~33% cholesterol (CHL) to each membrane model. This concentration is about the typical sterol concentration in the mammalian plasma membrane.[44] We also construct a model (M5) containing only 15% cholestrol, but where the numbers of lipids are the same as that of the M1 model. These two models M1 and M5 enable us to study the effect of the reduction in cholesterol concentration. The numbers of lipids and cholesterol for the five normal membrane models are listed in Table 1. As seen, the asymmetry of lipid distributions between two leaflets, which is

Table 1 Total number of each lipid component in the outer and inner leaflets of five normal cell membrane models. The models M1 and M2 are based on the work by Rivel *et al.*,[24] the model M3 is based on the work by Klahn *et al.*,[25] and model M4 is based on the work by Ingolfsson *et al.*[26] Model M5 is as same as model M1 but contains only half the cholesterol concentration

	M1		M2		M3		M4		M5	
Lipid	Outer	Inner	Outer	Inner	Outer	Inner	Outer	Inner	Outer	Inner
SM	84	24	76	12	90	6	56	28	84	24
DOPC	92	28	70	18	78	30	104	48	92	28
DOPE	28	92	38	110	28	100	18	70	28	92
DOPS	0	60	16	60	8	64	0	30	0	60
CHL	102	102	102	102	102	102	102	102	51	51

a general feature of normal membranes, is taken into account in the construction.

Having designed the normal membranes, the cancer counterparts are obtained by symmetrizing the number of lipids between the two leaflets. This mimics the overexpression in PS/PE in the outer leaflets of cancer membranes. The population of cholesterol is kept the same between the two leaflets. The number of lipids for the five cancer membrane models is listed in Table 2.

2.2 Simulation method

Given the number of lipids listed in Tables 1 and 2, we use the CHARMM-GUI platform to build the membranes. The all-atom CHARMM36 force field[45] and the TIP3P water model[46] are used to model the lipids and solvent, respectively. The initial dimensions of the unit cell are (L_x, L_y, L_z) = (12, 12, 9) nm. Starting from each initial structure, an equilibrium MD simulation is carried out for 100 ns, followed by a production run for 1000 ns in the *NPT* ensemble with a pressure P_0 = 1 bar and temperature T = 300 K. The GROMACS simulation package[47] is used for the simulation. The Berendsen coupling methods[48] are used to maintain the pressure and temperature of the system at the desired values with the coupling constants of 0.1 ps. The equations of motion are integrated using the leapfrog algorithm with a small time step of 2 fs. The electrostatic interactions are calculated using the particle mesh Ewald method and a cutoff of 1.4 nm.[49] A cutoff of 1.4 nm is used for the van der Waals interactions. The non-bonded pair lists are updated every 5 fs. The data are saved for every 10 ps for subsequent analyses.

2.3 Membrane elastic moduli

From the simulation data, we calculate the elastic moduli of membranes using the method recently developed by Levine *et al.*[31–33] It is useful to briefly describe the method here, and the readers are referred to ref. 31–33 for more details. First, the orientation of a lipid is characterised by a unit vector $\mathbf{n}^\alpha$, which points from the midpoint between the phosphorus and glycerol C2 atoms of the head group to the midpoint between the two terminal methyl carbons of two lipid tails. For cholesterol, the unit vector joins the C3 and C17 atoms [Fig. 1]. Here, α = 1 and 2 denote the lipids belonging to the outer and inner leaflets, respectively. Let $\mathbf{u}_r^\alpha(\mathbf{r})$, where $\mathbf{r} = \mathbf{r}(x, y)$, be the projection vector of the vector $\mathbf{n}^\alpha$ on the xy plane of the membrane, and $\mathbf{u}_q^\alpha(\mathbf{q})$ be the Fourier transform of $\mathbf{u}_r^\alpha(\mathbf{r})$. The orientation vector of the bilayer is then defined as $\mathbf{u}_q(\mathbf{q}) = [\mathbf{u}_q{}^1(\mathbf{q}) - \mathbf{u}_q{}^2(\mathbf{q})]/2$. This vector is then decomposed into a longtitudinal component $\mathbf{u}_q^\parallel = 1/q[\mathbf{q}\cdot\mathbf{u}_q]$ and a transverse component $\mathbf{u}_\mathrm{q}^\perp = 1/q[\mathbf{q} \times \mathbf{u}_q)]\cdot\hat{z}$. It has been shown that[31–33]

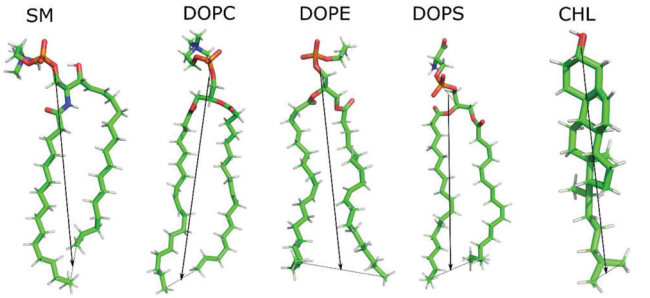

Fig. 1 Molecular structure of lipids and cholesterol used to construct the membranes in this work. The orientation of the lipid is described by the black unit vector. See text for detailed definition.

$$\left\langle |\mathbf{u}_q^\parallel|^2 \right\rangle = \frac{k_\mathrm{B}T}{K_\mathrm{c}q^2}, \quad \langle |\mathbf{u}_q^\perp|^2 \rangle = \frac{k_\mathrm{B}T}{K_\theta + K_\mathrm{tw}q^2} \tag{1}$$

where T is the temperature, k_B is Boltzmann;s constant, K_c, K_θ and K_tw are the bilayer bending, lipid tilt and twist moduli, respectively.

We also calculate the bending modulus K_c using the local real-space method of Khelashvili *et al.*[35] First, the potential of the mean force of the angle α between the two neighbouring lipid unit vectors $\mathbf{n}^\alpha$ is extracted from the simulation

$$U(\alpha) = -k_\mathrm{B}T \ln\left[\frac{P(\alpha)}{\sin(\alpha)}\right], \tag{2}$$

where $P(\alpha)$ is the probability distribution of α over all configurations, and all lipid pairs. A lipid pair is considered if two lipids are separated by less than 1 nm, and at least one unit vector is oriented $\leq$10 degrees from the bilayer normal. The splay modulus χ^{ij} between a pair of lipids is obtained by fitting the plot of eqn (4) to a functional form

$$U(\alpha) = \frac{1}{2}\chi^{ij}\alpha^2 + c, \tag{3}$$

where c is a constant, and the fit is limited to small values of α in a range of 10–30 degrees. The bending modulus K_c is then calculated as

$$\frac{1}{K_\mathrm{c}} = \frac{1}{\phi_\mathrm{total}} \sum_{\langle i,j \rangle} \frac{\phi_{i,j}}{\chi^{ij}}, \tag{4}$$

Table 2 Total number of each lipid component in the outer and inner leaflets of five cancer cell membrane models. Each cancer model M*i** (*i* = 1,. . .,5) is obtained by symmetrising the number of lipids between the outer and inner leaflets of the normal membrane model M*i* counterpart shown in Table 1

	M1*		M2*		M3*		M4*		M5*	
Lipid	Outer	Inner	Outer	Inner	Outer	Inner	Outer	Inner	Outer	Inner
SM	54	54	44	44	48	48	42	42	54	54
DOPC	60	60	44	44	54	54	76	76	60	60
DOPE	60	60	74	74	38	64	44	44	60	60
DOPS	30	30	38	38	16	36	16	16	30	30
CHL	102	102	102	102	102	102	102	102	51	51

where ϕ_{ij} is the number of i,j neighbouring pairs, and ϕ_{total} is the total number of ϕ_{ij} for all pairs.

3 Results

3.1 Structural properties

3.1.1 Lipid surface area. To obtain the first impression on the structural properties of the membranes, we calculate the average area occupied by individual lipids (area per lipid, A_L) pertaining to the outer and inner leaflets of each membrane model. We employ the method recently developed by Gapsys *et al.*,[50] which is based on the GridMAT-MD algorithm[51] and implemented using GROMACS as the analysis tool g_{lomepro}. The time evolution and histogram distribution of A_L for all membrane models are shown in Fig. S1 and S2 (ESI†). The results show that the structure of the membranes has relaxed to a reasonable state and is stable during the simulation timescale of 1 μs. The time average values of A_L listed in Table 3 indicate that although there are differences in the mole fraction of lipids between normal membranes, between cancer membranes, between two leaflets, or between normal and cancer membranes, the area per lipid values for all models are quite similar, lying in the range of $\sim$51.74–54.46 Å^2. This is a typical range of A_L for common lipid bilayers previously reported from experiments and atomistic simulations.[52] The area per lipid values of models M4 and M4* are somewhat lower than the other models. This is because M4 and M4* have low DOPS and DOPE concentrations [Tables 1 and 2]; moreover, the size of the serine group of DOPS, and of the ethanolamine group of DOPE, is smaller than the choline group of other lipids. At the lower cholesterol concentration of 15%, the area per lipid values of models M5 and M5* are higher than those of the M1 and M1* counterparts. This is because the presence of cholesterol in the lipid bilayer increases the free spaces between the lipid chains,[53] thus effectively decreasing the lipid area in M1 and M1*. This effect of cholesterol was also observed in the MD simulations of Klahn *et al.*[25] and Shahane *et al.*[52] for their cancer membrane models. Overall, our results show that the area per lipid does not depend much on the model used, it is not affected much by the overexpression of the DOPS lipid in the outer leaflet, but it is increased as the cholesterol concentration decreases.

Table 3 Area per lipid (A_L) and the thickness (d) of the normal (M1···M5) and cancer (M1*···M5*) membranes. The area per lipid is shown for the outer and inner leaflets. The data shown are results averaged over 1 μs trajectories at 300 K

	A_L [Å^2]		
Membrane model	Outer	Inner	d [Å]
M1	54.24 ± 0.13	54.30 ± 0.17	42.6 ± 0.3
M1*	54.28 ± 0.14	53.95 ± 0.14	42.7 ± 0.3
M2	53.90 ± 0.16	53.82 ± 0.12	42.6 ± 0.3
M2*	54.20 ± 0.13	54.46 ± 0.13	42.4 ± 0.2
M3	53.68 ± 0.14	54.19 ± 0.13	42.7 ± 0.4
M3*	54.34 ± 0.13	54.13 ± 0.12	42.5 ± 0.3
M4	51.74 ± 0.15	51.94 ± 0.11	42.3 ± 0.4
M4*	52.48 ± 0.11	52.27 ± 0.14	42.2 ± 0.2
M5	56.27 ± 0.19	56.39 ± 0.18	41.6 ± 0.2
M5*	55.99 ± 0.18	56.24 ± 0.16	41.8 ± 0.2

3.1.2 Electron density and membrane thickness. To understand the effects induced by the overexpression of the negatively charged DOPS lipids in the outer leaflet of the cancer cell membranes, we calculate the electron density of the normal and cancer cell membrane models along the z-dierection, and the results are shown in Fig. 2. As seen, the electron density profiles of the membrane for the models M1···M4 and M1*··· M4*, which have the same cholesterol concentration of 33%, are not significantly different. Thus, the membrane thickness, which is measured as the distance between the two maxima of the average electron density in the z-direction, for all models is also quite similar, $\sim$4.2 nm [Table 3], which agrees with previous results of experiments,[17] and simulations.[25,52] The reduction of the cholesterol concentration in models M5 and M5* results in a slight decrease ($\lesssim$10%) in the thickness. This is because an increase in cholesterol causes a decrease in the lipid surface area, and because a lipid membrane behaves as an incompressible fluid, thus the bilayer thickness is increased. In all cases, the time evolution of the thickness of all membranes undergoes some fluctuations within the first 400 ns before relaxing to a stable value, indicating the convergence of the simulations [Fig. S3 and S4, ESI†]. We also calculate the electron density of the sodium cations and chloride anions in the direction perpendicular to the membrane for all models, and the profiles are also shown in Fig. 2. Due to the asymmetry in the distribution of lipids in normal membranes, the interactions of the outer and inner leaflets with ions are different, resulting an asymmetry in the profiles, with a low and and high density of sodium on the outer ($z \geq 5$ nm) and inner ($z \leq 5$ nm) leaflets, respectively. By contrast, the densities of chloride are high and low on the outer and inner leaflet, respectively. The increase of the negatively charged DOPS lipids in the outer leaflet of the cancer membranes results in the increase and decrease of the sodium and chloride concentration on the surface of that leaflet, respectively. This was also observed in the simulations of Klahn *et al.*[25], whose membrane models are similar to our M3, M3* models. Due to the difference in the lipid mole fractions between normal cell membrane models, or between cancer cell membrane models, there are slight differences in the peaks of the density profiles of the ions. For example, the peak of the sodium profile is about 3 e nm^{-3} for M1 but only 2 e nm^{-3} for M3 at $z \geq 1.5$ nm. A comparison of the model M1 (M1*) with the counterpart M5 (M5*) shows that a change in the cholesterol concentration does not lead to significant changes in the electron density of the membranes as well as of the ions. Overall, our simulations show that the electron density profiles of the lipid bilayers are similar for all membrane models, regardless of the difference in the lipid and cholesterol concentrations, but the electron densities of the ions on the membrane surfaces depend slightly on the membrane models and differ between normal and cancer cell membranes.

3.1.3 Lipid order parameters. Next, we wish to understand whether or not the ordering of the lipid acyl chain tails depends

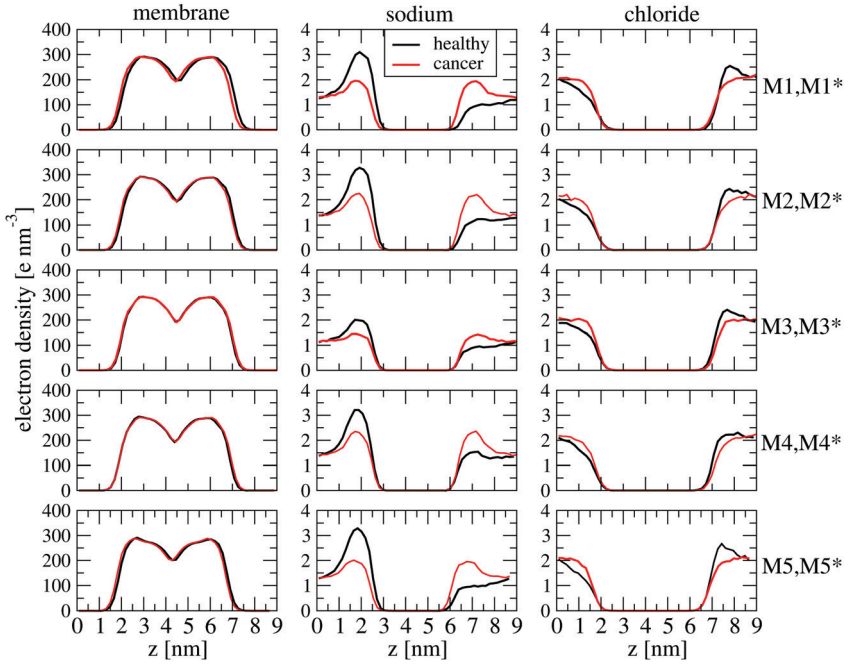

Fig. 2 Electron density profile of the lipid membrane (left panels), the sodium ions (middle panels) and chloride ions (right panels) along the z-direction. Shown are results for normal (black) and cancer (red) cell membranes.

on the membrane models, and exhibits any difference between the normal and cancer cell membranes. Here, an order parameter is defined as $S_{CH} = \langle 3\cos^2\ \theta - 1\rangle/2$, where θ is the angle between a C–H bond vector and the bilayer normal.[54] The angular brackets represent molecular and temporal ensemble averages. The values of S_{CH} vary between 1, where all the CH_2 groups form a straight line, and 0, if all possible angles θ are found with the same probability. For the DOPC, DOPE and DOPS lipids, each tail consists of 17 order parameters, and for SM lipids, each tail consists of 15 order parameters. We find that the order parameters of the lipids in all models are very similar, and Fig. 3 shows, as examples, the results of the M1, M1* models and theirs lower-concentration cholesterol counterparts M5, M5*. As seen, the values are superposable between

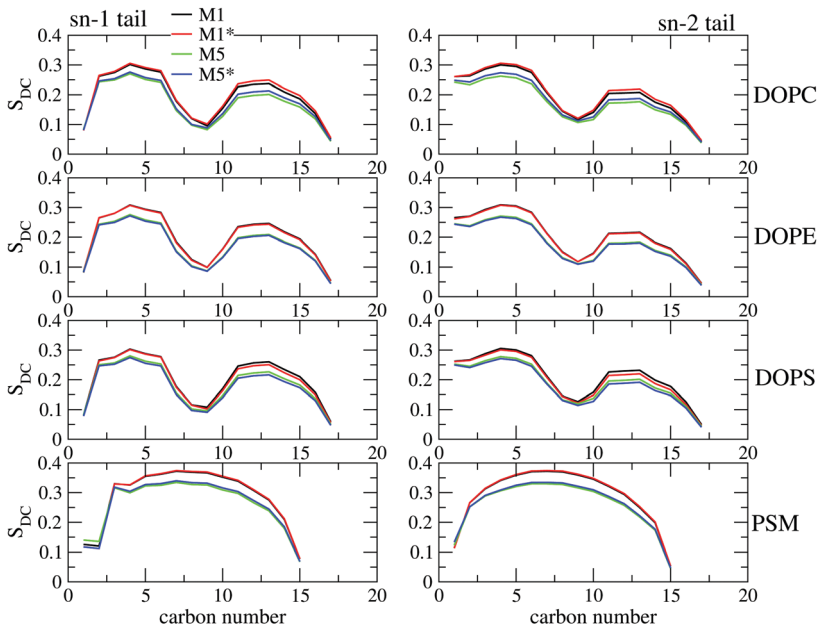

Fig. 3 Comparison of the order parameters for the two tails sn-1 (left) and sn-2 (right) for four lipid types, DOPC, DOPE, DOPS and SM, of the normal (M1, M5) and cancer (M1*, M5*) cell membrane models. The carbon atom numbers increase in the direction of the tail termini. The results shown are averaged over 1000 ns trajectories at 300 K.

the normal and cancer cell models M1, M1* or M5, M5*, and they are also similar to those reported in the literature.[54] It is known that the presence of cholesterol in the lipid membrane increases the ordering of lipid chains,[53] and this is also seen from our simulations, showing that the lipid order parameters of M5 or M5* are lower than those of the M1 or M1* models. Overall, the results indicate that the lipid orientational order does not sensitively depend on the difference in the lipid mole fractions of the models, regardless of whether they are normal or cancer cell types, and on the overexpression of the DOPS lipids in the outer leaflet, but does decrease with the decrease in the cholesterol concentration.

3.1.4 Membrane electrostatic potential. The electrostatic potential across the membrane $\Psi(z)$ is related to the charge density $\rho(z)$ along the membrane normal z *via* the Poisson equation

$$\frac{\mathrm{d}^2\Psi(z)}{\mathrm{d}z^2} = -\frac{\rho(z)}{\varepsilon_0}. \tag{5}$$

Here, ε_0 is the electrostatic permittivity of a vacuum. Because the simulations have been done using periodic boundary conditions, thus we impose the condition $\Psi(0) = \Psi(L)$, where L is the simulation box length in the z-direction. By choosing $z = 0$ at the corner of the simulation box and setting $\Psi(0) = 0$, the potential can be calculated as[55]

$$\Psi(z) = -\frac{1}{\varepsilon_0}\int_0^z (z-t)\rho(t)\mathrm{d}t + \frac{z}{\varepsilon_0 L}\int_0^L (L-t)\rho(t)\mathrm{d}t. \tag{6}$$

In practice, the charge density $\rho(z)$ is calculated by dividing the whole box into 500 slabs of 0.018 Å parallel to the x–y plane and counting the number of charges in each slab. As an example, Fig. 4(A) shows the charge density profile of the normal and cancer cell membranes M1 and M1*. The dominant positive peak in the outer leaflet at $z \approx$ 7–7.5 nm of M1 is mainly contributed by the positively charged choline groups of highly populated DOPC and SM lipids. The negative peaks at $z \approx$ 6.5–7 nm (outer leaflet) and $z \approx$ 2–2.5 nm (inner leaflet) are similar, and both come from the negatively charged phosphate groups of DOPC, DOPE and SM lipids. Due to the high population of DOPS lipids in the inner leaflet of the normal cell membranes, their negatively charged serine groups compensate with the positively charged groups of DOPC, DOPE, and SM, leading a low peak in the profile at $z \approx$ 1–1.5 nm. As expected, the charge profile of the cancer cell membrane M1* is symmetric due to the symmetry of the two leaflets. For both membranes, the peaks at the membrane center are quite high, and come mainly from the partial charges on the terminal methyl group at the lipid tails. Fig. 4(B) shows the potential obtained from eqn (6) with the density from Fig. 4(A). Due to high negative density in the inner leaflet of M1, the electrostatic potential in this leaflet is more negative than that in the outer leaflet. Again, the potential profile of M1* is symmetric between the two leaflets, with peaks being higher and lower than that of M1 in the inner and outer leaflets, respectively. The charge density and electrostaic potential profiles of the other normal or cancer cell models show similar behaviour to that of M1 or M1*. Overall, our simulation shows that the electrostatic potential of the normal cell membrane is asymmetric, with a downhill slope on going from the outer leaflet to the inner leaflet. By contrast, the electrostatic profile of the cancer cell membrane is symmetric and rather flat. This indicates that the electrostatic potential is indeed affected by the overexpression of the DOPS lipid in the outer leaflet of the cancer cell membrane.

3.2 Membrane elastic properties

Having compared the normal and cancer cell membranes in terms of structural properties, in the following we compare their elastic properties. From our simulation data, we extract the orientation vectors $\mathbf{u}_r^\alpha$ of the lipid and cholesterol molecules, and the power spectra as a function of the wavelength q

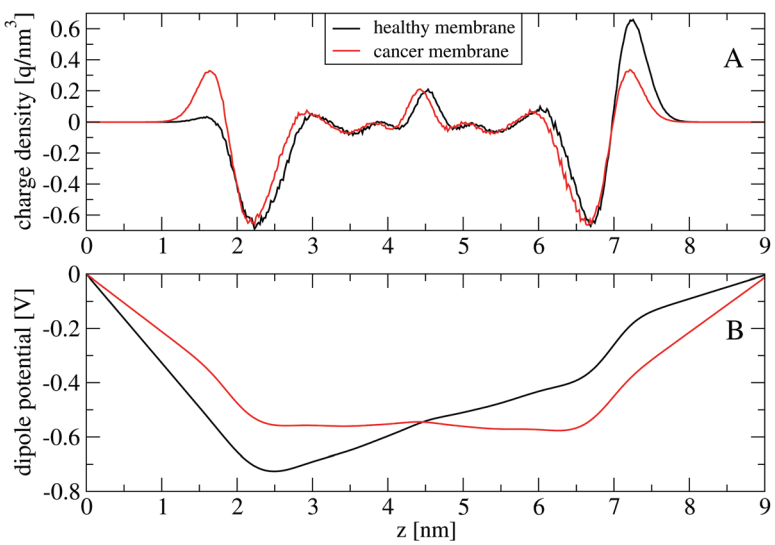

Fig. 4 Charge density (A) and the dipole potential (B) profiles along the z-direction. Shown are the results of the normal (black) and cancer (red) cell membrane models M1 and M1*.

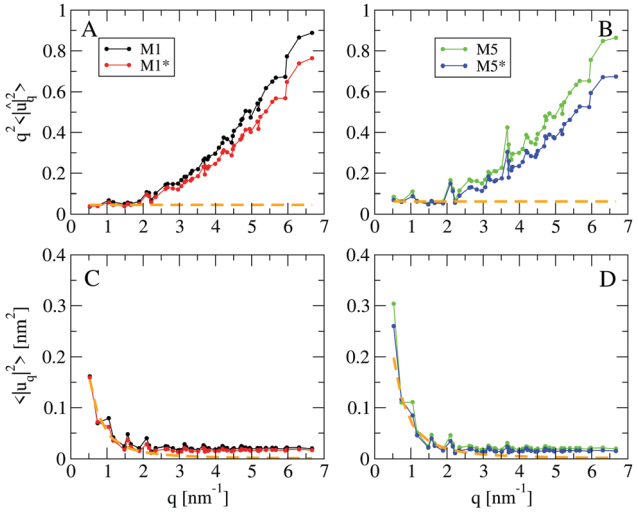

Fig. 5 Power spectra of the longitudinal (weighted by q^2) (A and B) and transverse (C and D) components of the lipid orientation vector. Shown are the results of the high-concentration cholesterol membrane models M1, M1* (A and C) and low-concentration cholesterol membrane models M5 and M5* (B and D). The best fits of the data to eqn (1) are shown by the orange dashed lines. Only data points in the range $0 < q < 1.5$ nm^{-1} are used for the fit of the longitudinal curves, and $0 < q < 3.5$ nm^{-1} for the transverse curves. The spectra are averaged over 1000 ns trajectories.

are calculated from eqn (1). The spectra are averaged over 1000 ns, and are shown in Fig. 5, as an example, for the M1 and M1* models. As seen, the spectra $\langle|\mathbf{u}_q^{\parallel}|^2\rangle$ (weighted by q^2) are almost constant with $q < 1.5$ nm^{-1} or equivalently $r > 2\pi/q \approx 4.2$ nm [Fig. 5(A and B)]. In this plateau region the theoretical prediction for K_c, eqn (1), is valid, and this allows us to extract the constant K_c by fitting the data points to a straight line [Fig. 5(A and B)]. Note that the plateau region extends over the distances $r > 4.2$ nm, which is much smaller than the length of the simulation box of 12 nm, and thus the results of K_c are well-converged with the system size. This is an advantage of the fluctuation method, which does not require a large system size as mentioned by Levine *et al.*[33] To obtain the tilt (K_θ), and twist (K_{tw}) moduli, we fit the power spectra shown in Fig. 5(C and D) to the theoretical prediction curve, eqn (1). Here, only data points with $0 < q < 3.5$ nm^{-1} are used for the fitting. The elastic moduli of all normal and cancer cell membranes at 300 K are listed in Table 4. The error bars are estimated using five data blocks, each of 200 ns.

We first compare the elastic moduli between the normal cell membrane models, or between the cancer cell models at the cholesterol concentration of 33%. To this end, we calculate the variation in each elastic modulus between any two normal cell membranes, or between any two cancer cell membranes. We find that, within the error bars, the values of the bending modulus K_c of all normal cell membranes or all cancer cell membranes are basically the same. For the tilt and twist moduli, the largest variation is 10% for K_θ between M2 and M3, and 25% for K_{tw} between M3 and M4. The maximum differences between the cancer cell membrane models are 15% for K_θ of the pair M1*–M2*, and 26% for K_{tw} of the pair M3*–M4*. These differences are more or less in the same order of the largest error bars, which are 12% for K_θ of M1, 7% for K_{tw} of M1, 15% for K_θ of M1*, and 7% for K_{tw} of M4*, indicating that the tilt and twist elastic moduli are also similar between models, regardless of the normal or cancer cell membrane type.

Table 4 Bending (K_c), tilt (K_θ) and twist (K_{tw}) elastic moduli of the normal (M1···M5) and cancer (M1*···M5*) cell membrane models calculated using eqn (1). The bending modulus K_c' is calculated using eqn (4). Shown are the results at a temperature of 300 K obtained using the analysis of the fluctuation of the lipid orientation vector method. The error bars are obtained using the block average method with 5 data blocks, each 200 ns long

Model	K_c (10^{-20} J)	K_θ (10^{-20} J nm^{-2})	K_{tw} (10^{-20} J)	K_c' (10^{-20} J)
M1	10.5 ± 0.7	4.2 ± 0.5	1.3 ± 0.1	10.33 ± 0.8
M1*	10.6 ± 0.8	4.0 ± 0.6	1.6 ± 0.1	10.29 ± 0.8
M2	11.5 ± 0.3	4.3 ± 0.3	1.5 ± 0.1	10.32 ± 0.9
M2*	11.9 ± 0.4	4.6 ± 0.7	1.6 ± 0.1	10.25 ± 0.9
M3	9.5 ± 0.6	3.9 ± 0.3	1.2 ± 0.1	10.32 ± 0.6
M3*	9.7 ± 0.7	4.4 ± 0.4	1.9 ± 0.1	10.31 ± 1.2
M4	10.2 ± 0.8	4.2 ± 0.3	1.6 ± 0.1	10.21 ± 0.9
M4*	10.6 ± 0.5	4.1 ± 0.4	1.4 ± 0.1	10.24 ± 0.8
M5	8.2 ± 0.5	1.3 ± 0.2	0.8 ± 0.1	9.87 ± 0.5
M5*	8.1 ± 0.4	1.2 ± 0.2	0.9 ± 0.1	9.84 ± 1.0

A comparison of the normal cell membranes with cancer cell membranes reveals that within the error bars, there are basically no differences in the bending (K_c) and tilt (K_θ) moduli of any transformations Mi → Mi*. However, there is a small difference in K_{tw}, that is, M1*, M2* and M3* are about 23%, 7% and 58% stiffer than M1, M2, and M3, respectively, but M4* is 12% softer than M4. At a lower cholesterol concentration of 15%, the models M5 and M5* have similar bending and tilt moduli, but the twist mode of M5* is about 25% stiffer than that of M5.

A comparison between the cell membranes with different cholesterol concentrations shows that all elastic moduli of the membranes with low cholesterol are smaller than those of membranes with high cholesterol. The normal cell membrane model M5 is ∼22%, 69% and 38% softer than M1 in the bending, tilt and twist modes, respectively. The cancer cell membrane model M5* is ∼24%, 70% and 43% softer than M1* in the bending, tilt and twist modes, respectively. All of the above results show that if we consider the cancer model M5* as a transformation of the normal model M1, then it is clear that the softening in the elastic modulus of M5* is mainly caused by the reduction in the cholesterol concentration, but not by the overexpression of the DOPS lipid in the outer leaflet.

We also calculate the bending modulus K_c of all membrane models using the real-space method of Khelashvili *et al.*,[35] and the results shown in Table 4 indicate that, for each membrane model, there is essentially no difference in the bending modulus obtained using the two methods. The differences are less than 10%, except where the largest difference is about 17% for the M5 or M5* models. This confirms that our results are not strongly biased due to the calculation methods used. We note that while the method by Levine *et al.*[33] shows clearly the effect of the cholesterol concentration, the results obtained using the

method of Khelashvili *et al.*[35] are not clearly evident. Nevertheless, both methods do show a trend that K_c is smaller at the lower cholesterol concentration.

Overall, the results show that with the same cholesterol concentration but with a difference in the lipid mole fractions, the bending and tilt moduli of the different membranes, regardless of whether normal or cancer cell types, are very similar. However, there are small differences in the twist modulus between normal cell membrane models, between cancer cell membrane models, or between normal and cancer cell membranes. The reduction in cholesterol concentration clearly yields a low elastic modulus, *i.e.*, softening in the membranes. This is because changes in the cholesterol concentration can affect both the phase behaviour[16] and phase separation[56] in lipid membranes, thereby altering, respectively, both globally[57,58] and locally,[57,59] the mechanical properties of the cell membranes.

3.3 Discussion

It has been suggested that cancer cells are generally softer than their normal counterparts. Several extracellular and intracellular factors could contribute to that mechanical difference.[2] In this work, we employ atomistic MD simulations to examine whether or not there are any differences in the structure and elastic properties of normal and cancer cell membranes.

While the MD simulation methods of lipid membranes are well-established, it is clear that the simulation results could depend on the computational membrane models. Although biological membranes are very complex entities that contain many distinct lipid species, to be computationally feasible, most computational models include only representative lipids. Both the normal and cancer cell membranes of this work contain four types of lipid – DOPC, DOPE, DOPS, SM – and cholesterol. The cancer cell membranes are constructed from normal cell membranes based on two fundamental transformations that are usually observed in cancer cell membranes: the overexpression of the PS lipid population in the outer leaflet, and the reduction of the cholesterol concentration. It is clear that these models have two main limitations: they cannot represent the cell membrane of various types of cancer cell, and other transformations are not included. For example, an increase in microvilli, which leads to large cell surfaces and the total amount of lipids,[60,61] is not considered in the models. In addition, the symmetrization of the lipid populations between the outer and inner leaflets of our cancer membrane models is oversimplified, because in reality the cancer cell membranes are likely to remain somewhat asymmetric. Therefore, to obtain statistically reliable results, we consider several membrane models in this work, and their results are discussed in the following.

In a previous study, Rivel *et al.* used different cell membrane models to compare the permeability of the anti-cancer drug cisplatin through the normal and cancer cell membranes using MD simulations.[24] Our normal cell models M1, M2 and cancer cell models M1*, M2* are constructed using the same lipid mole fractions as the models of Rivel *et al.* However, our models are larger to avoid the finite-size effect in the calculation of the elastic moduli. We note that Rivel *et al.*[24] employed the umbrella enhanced sampling technique with the total sampling of 0.5 μs to guarantee the sampling convergence of the simulations, while our MD simulations are longer, at 1 μs. Nevertheless, both simulations show that, given the same cholesterol concentration, various structural quantities, such as the area per lipid, the membrane thickness [Table 3], the density profile [Fig. 2], and the lipid order parameters [Fig. 4] of the normal and cancer cell membranes, are almost identical. This implies that the finite-size effect is negligible, and the conformational sampling of our simulations is reasonable.

Our normal cell model M3 is constructed using the same mole fractions of lipids as the model of Klahn *et al.*,[25] but again the size of our model is larger. The cancer cell membrane model of Klahn *et al.*[25] takes into account two main changes, *i.e.*, an increase in PS lipids in the outer leaflet and a decrease in the cholesterol concentration, but the mole fractions of the other lipids in the two leaflets are very similar, *i.e.*, the cancer cell membrane remains somewhat asymmetric. By contrast, our cancer membrane model M3* is symmetric with the same lipid populations in the two leaflets [Table 2]. Despite the differences, their simulations and our results for M3, M3* show that the structural properties [Fig. 2 and 4] of the normal and cancer cell models are almost identical. This suggests that the simple symmetrization of the lipid distributions in the construction of our cancer cell membrane models does not affect the results.

Our normal cell model M4 is constructed using the same mole fractions of lipids as the realistic mammalian cell membrane models developed by Ingolfsson *et al.*[26] The cancer cell counterpart M4* is obtained *via* symmetrization of the distribution of lipids between the two leaflets of M4 [Table 2]. The models of Ingolfsson *et al.* are very complex, consisting of different lipid species, combining different types of head group and different types of tail asymmetrically distributed across the two leaflets. However, their MD simulations using the coarse-grained MARTINI force field show striking similarities in the overall bilayer properties, such as the bilayer thickness, lipid tail order, diffusion, flip-flop, and average neighbours, despite the significant difference in lipid compositions between the two models. Our all-atom simulations show that the structural properties of M4 and M4* are quite similar. These results may suggest that use of the coarse-grained MARTINI or all-atom CHARMM36 force field should not yield significant differences in the overall bilayer structural properties.

As mentioned above, Rivel *et al.* used cell membrane models, which are similar to our M1 and M1* models, to compare the permeability of the cisplatin drug through normal and cancer cell membranes.[24] Although the structural properties are similar, the authors observed that the loss of lipid asymmetry in the cancer cell membranes leads to a decrease in their permeability to cisplatin by one order of magnitude in comparison with the asymmetric membranes of normal cells. To explain this observation, the authors calculated the diffusion constant, and showed that the diffusion of cisplatin is slower in the cancer cell membrane than in the normal

counterpart, although the energy barrier of permeation remains the same in both membranes.[24] Our simulations show that due to the asymmetric distribution of charged lipids between the inner and outer leaflets, the electrostatic potential of the normal cell membrane is asymmetric, with a downhill slope in the potential on going from the outer leaflet to the inner leaflet [Fig. 4]. This potential gradient could accelerate the diffusion of cisplatin from the outer to inner leaflets. By contrast, the electrostatic profile of the cancer cell membrane is symmetric and rather flat, resulting in the slow diffusion of cisplatin. In this context, we believe that changes in the electrostatic potential in going from normal to cancer cell membranes may change the interaction between cancer cells with their surroundings, leading to changes in the elastic properties, whether softer or harder cancer cells. However, this hypothesis needs to be studied further.

Concerning to the elastic moduli, the question is whether or not the calculated results depend on the employed method? As mentioned, the analysis of fluctuation of the lipid orientation vector using the Fourier-space[31–33] method and the real-space method[35] are currently widely used. It has been demonstrated that these two methods yield similar results with a difference of up to 17% for the different pure membrane models DPPC, DOPC and DOPE (see the supporting information of ref. 33). Allolio *et al.* also calculated the elastic moduli of a large variety of systems, including mixtures and curved cell membrane geometries, using both the real-space and Fourier analysis methods. The authors found good agreement between the two methods.[36] Nevertheless, in addition to the results presented above obtained from the fluctuation analysis in the Fourier space, we also calculated the elastic bending modulus using the real-space method of Khelashvili *et al.*,[35] and as shown in Table 3, the results of both methods are in good agreement. This indicates that our results are not biased due to the employed calculation methods, in agreement with the findings of Allolio *et al.*[36]

Due to the lack of experimental data, a direct comparison of our simulation results with experimental elastic moduli of multiple-component lipid membranes is unfortunately impossible. Recently, Venable *et al.* carried out atomistic MD simulations for 12 fully hydrated single-component bilayers.[34] Encouragingly, the values of the bending modulus K_c, calculated using eqn (1), were in near-quantitative agreement with vesicle flicker experiments. Notably, an excellent agreement between simulation and experiment was obtained for DOPE membrane. This encouraging result gives us confidence that the elastic moduli of our membrane models will also be close to that of real membranes, although the results are not directly compared to experiments. This suggests that the simulation approach could be useful to study the mechanical properties of cell membranes, and in particular, to compare the elastic properties of the normal and cancer cell membrane models.

In this work, we focus on effects of the overexpression of the DOPS lipid in the outer leaflet as well as the reduction of cholesterol concentration on the elastic moduli of cancer cell membranes. In our cell membrane models, the mole fraction of the DOPS lipid was taken from the lipid content of mammalian erythrocyte membranes measured *via* experiments,[41–43] and the mole fraction of CHL is about the typical sterol concentration in the mammalian plasma membrane.[44] The simulations show that (i) given the same cholesterol concentration, there is no clear evidence to show that the cancer membranes are softer than their normal counterparts. That is, the bending and tilt elastic moduli of the normal and cancer cell membranes are similar, and the twist modulus of a cell cancer membrane could be slightly softer than that of the normal counterpart or *vice versa*. This indicates that the overexpression of DOPS lipid in the outer leaflet may not be an essential factor that directly causes softening of the cancer cells, but rather is a biological cue related to the apoptotic pathway. As shown, however, the electrostatic potential of the membrane is altered due to the redistribution of PS lipids, and this could alter the interaction between the cells with their surroundings, thus resulting in indirect changes in the elasticity of cancer cells. (ii) If the cholesterol concentration is reduced, then all elastic moduli of normal cell membranes are reduced, regardless of whether there is an overexpression in DOPS lipids in the outer leaflet (M1 → M5*) or not (M1 → M5). To explain this effect of cholesterol, we note that for a long time cholesterol has been known to stiffen saturated lipid membranes, and recently, Chakraborty *et al.* have shown that cholesterol also increases the bending rigidity of unsaturated lipid membranes.[62–64] This suggests that cholesterol should also stiffen membranes that are made up of a mixture of saturated and unsaturated lipids, which is the case for our membrane models. In this context, the reduction in cholesterol is one of the factors that causes the softening of cancer cell membranes. We should mention that the effect, which is caused by cholesterol on the structure of membranes, has been observed in both experiments and simulations for various bilayer membrane systems.[13–17] However, we have studied, for the first time, this effect on the elasticity properties of normal and cancer cell membranes in this work. We note that the mole fraction of DOPS lipid in the outer leaflet is increased by ~5–12% upon transforming from normal to cancer cell membranes [Tables 1 and 2]. In a previous study, Doktorova *et al.* carried out the MD simulations of a mixed POPC/POPS membrane containing 30% PS in each leaflet. The authors showed an opposite effect, that is, the bending modulus of the POPC/POPS membrane is 22% larger than that of the pure POPC membrane.[37] This is consistent with the theoretical consideration, which predicts an increase in the bending rigidity in the presence of charged lipids due to electrostatic repulsion between the lipid headgroups.[65,66] However, Jiang *et al.* recently carried out MD simulations of a pure POPC lipid membrane, and a mixed POPC/POPS membrane containing 20% POPS only in the inner leaflet. The simulations showed that the bending modulus of the POPC/POPS membrane is ~20% smaller than that of the POPC membrane.[38] This finding was explained by the fact that the overall effect of POPS lipids on the bending modulus depends largely on the number of POPS lipid pairs, as seen from eqn (4). Thus, high mole fractions of PS are required to observe a

significant effect on the bending modulus. In our membrane models, the mole fraction of the DOPS lipid is rather low, ~5–12%, thus any effect due to the overexpression of DOPS lipid in the outer leaflet on the elastic moduli is not evident.

The remaining question is whether or not our results can be related to the experimental measurement of the softening of cells? Several experimental techniques, such as atomic force microscopy (AFM),[5] micropipette aspiration[4] and particle-tracking microrheology,[3] have been developed to measure the stiffness of cells. However, the results obtained from these methods are usually inconsistent. This is probably due to the fact that each method measures different cell components. In AFM experiments, the applied force is the sum of forces from the cell membrane, cytoskeleton network, and cytosol. In the micropipette aspiration method the cell membrane and cytoskeleton influence the results, and in the particle-tracking microrheology method the contribution of the cytoskeleton network is important. This fact indicates that all three components, including the cell membrane, cytoskeleton network, and cytosol, contribute to the stiffness of the cells. The cytoskeleton has long been considered to be the main factor that affects the cell stiffness,[67] and this has motivated some researchers to try to adjust the cell stiffness by regulating actin microfilaments.[68] Very recently, Ren *et al.* developed a physical model to analyze the AFM force relaxation curves, and showed that the softening of cancer cells is mostly due to the decrease of the membrane surface tension.[69] In a traditional AFM experiment, the membrane tension, σ, is estimated by measuring the force required to pull a membrane tether with radius of R_0 from the bilayer membrane. It has been shown that σ is approximately related to the membrane bending modulus K_c as $\sigma = K_c/2R_0^2$.[70] This implies that, according to the study of Ren *et al.*, the softening of cancer cells is mainly due to the decrease of the membrane bending modulus. In this context, the reduction of the cholesterol concentration in the cancer cell membranes, which reduces the bending modulus K_c, may contribute, at least in part, to the softening of the cancer cells, relative to the normal cells.

The present study has some limitations of which we are fully aware. First, for lipid mixtures like those of our models, the coupling between compositions is a possible driving force for the formation of lipid rafts.[71] Although our simulation time is rather long (1 μs for each system), it seems unlikely that lipids are perfectly ideally mixed. This non-ideality could affect the local shape and density, which in turn affects the elasticity properties of the cell membrane. Nevertheless, as we already mentioned that our MD simulations and enhanced sampling simulations of Rivel *et al.*[24] give similar results on the structural properties of both normal and cancer cell models, we believe that the effect due to limitation of sampling on the elasticity of the membranes should be minor. Second, in reality, a cell membrane is populated with ensembles of membrane proteins, thus the effective elastic moduli of a membrane are contributed by both the elastic properties of the lipid bilayer and of the proteins embedded within it.[72] Simulations of large complex lipid/proteins are infeasible at the moment, but will be pursued in future studies to investigate this hypothesis. Third, our cell membrane models have the same number of lipids in each leaflet, therefore, the area per lipid for the two leaflets are essentially forced to be the same. By contrast, the biological membrane in reality can have different numbers of lipids in each leaflet, therefore, the area per lipid for the two leaflets can be different, and thus the membrane can be curved, resulting in differences in the thickness and mechanical properties between the two leaflets. Indeed, Yesylevskyy *et al.* have recently carried out atomistic MD simulations to study the influence of the membrane curvature on the structural properties of the asymmetric membranes, and they showed that the thickness, the order parameter of the lipid tails and A_L are different between the two leaflets.[73] Whether or not the elastic moduli of the two leaflets of the curved membranes are different requires further investigation.

4 Conclusion

We have carried out all-atom MD simulations of five normal cell membrane models and five cancer cell membrane models. The cancer cell membranes are constructed taking into account the overexpression of the DOPS lipids in the outer leaflet and the reduction of the cholesterol concentration. Various structural quantities, including the area per lipid, the membrane thickness, the electron density, and the order parameters of the lipid tails, are calculated for each cell membrane. Results show that at the same cholesterol concentration all these quantities are very similar between the membranes, regardless of whether for normal or cancer cell models. This indicates that the overexpression of the DOPS lipids in the outer leaflet does not significantly affect the structure of the normal or cancer cell membranes. The effect of cholesterol is more pronounced in both cell membrane types, showing that if the cholesterol concentration is reduced then the area per lipid becomes larger, the cell membrane thickness is smaller and the lipid chains are more disordered. We find that the electrostatic potential of the normal cell membrane is asymmetric with a downward slope when going from the outer to the inner leaflet. Meanwhile, the potential energy of the cancer cell membrane is symmetrical between the inner and outer leaflets. Therefore, the molecular transport across the bilayer could be different between the normal and cancer cell membranes, and this may cause indirect differences in the mechanical properties of the two cell membrane types.

The elastic moduli of each membrane, including the bending, tilt and twist constants, are calculated using two different methods, and results of these two methods are quite similar. At the same cholesterol concentration, the bending and tilt moduli of the normal and cancer cell membranes are very similar. However, the twist modulus of the cancer cell membranes could be slightly larger or smaller than that of the normal cell counterparts, depending on the model. Nevertheless, since only the bending modulus contributes significantly to the stiffness of the bilayers, thus our results imply that there is no clear

evidence to indicate that the cancer cell membranes are softer than the normal cell counterparts. Thus, we conclude that the overexpression of the DOPS lipids in the outer leaflet also does not significantly affect the elasticity properties of cancer cell membranes. However, it will be of interest to see if there is any noticeable effect, of either an increase or a decrease in the bending rigidity of our cell membrane models due to the overexpression of the DOPS lipids, by increasing the DOPS mole fractions in the models. This work is underway. Finally, we show that at low cholesterol concentrations, all three elastic moduli become smaller, implying that the reduction in cholesterol concentration in cancer cell membranes could contribute partly to the softening of cancer cells.

Conflicts of interest

There are no conflicts to declare.

Acknowledgements

This work has been supported by the Department of Science and Technology at Ho Chi Minh City, Vietnam (grant 13/2020/HD-QPTKHCN), the ''Initiative d'Excellence'' program from the French State (Grant ''DYNAMO'', ANR-11-LABX-0011-01), the CNRS, the Narodowe Centrum Nauki, the National Science Foundation (NSF, grant SI2-SEE-1534941), the National Institutes of Health (NIH K25AG070277) and the CINES/TGCC/IDRIS centers for providing computer facilities.

References

1 C. B. Blackadar, Historical review of the causes of cancer, *J. Clin. Oncol.*, 2016, **7**, 54.
2 C. Alibert, B. Goud and J. B. Manneville, Are cancer cells really softer than normal cells?, *Biol. Cell.*, 2017, **109**, 167.
3 D. Wirtz, Particle-tracking microrheology of living cells: principles and applications, *Ann. Rev. Biophys.*, 2009, **38**, 301.
4 R. M. Hochmuth, Micropipette aspiration of living cells, *J. Biomech.*, 2000, **33**, 15.
5 Y. Ding, J. Wang, G. Xu and G. F. Wang, Are elastic moduli of biological cells depth dependent or not? Another explanation using a contact mechanics model with surface tension, *SoftMatter*, 2018, **14**, 7534.
6 D. Marquardt, B. Geier and G. Pabst, Assymmetric lipid membranes: towards more realistic model systems, *Membranes*, 2015, **5**, 180.
7 J. Connor, C. Bucana, I. J. Fidler and A. J. Schroit, Differentiation-dependent expression of phosphatidylserine in mammalian plasma membranes: quantitative assessment of outer-leaflet lipid by prothrombinase complex formation, *Proc. Natl. Acad. Sci. U. S. A.*, 1989, **86**, 3184.
8 T. Utsugi, A. J. Schroit, J. Connor, C. D. Bucana and I. J. Fidler, Elevated expression of phosphatidylserine in the outer membrane leaflet of human tumor cells and recognition by activated human blood monocytes, *Cancer Res.*, 1991, **51**, 3062.
9 R. A. Cruciani, J. L. Barker, M. Zasloff, H. C. Chen and O. Colamonici, Antibiotic magainins exert cytolytic activity against transformed cell lines through channel formation, *Proc. Natl. Acad. Sci. U. S. A.*, 1991, **88**, 3792.
10 W. F. Wonderlin, K. A. Woodfork and J. S. Strobl, Changes in membrane potential during the progression of MCF-7 human mammary tumor cells through the cell cycle, *J. Cell. Physiol.*, 1995, **165**, 177.
11 A. A. Gurtovenko and I. Vattulainen, Membrane potential and electrostatics of phospholipid bilayers with asymmetric transmembrane distribution of anionic lipids, *J. Phys. Chem. B*, 2008, **112**, 4629.
12 K. Simons and E. Ikonen, How cells handle cholesterol, *Science*, 2000, **290**, 1721.
13 E. Oldfield, M. Meadows, D. Rice and R. Jacobs, Spectroscopic studies of specifically deuterium labeled membrane systems. Nuclear magnetic resonance investigation of the effects of cholesterol in model systems, *Biochemistry*, 1978, **17**, 2727.
14 J. A. Urbina, S. Pekerar, H. Le, J. Patterson, B. Montez and E. Oldfield, Molecular order and dynamics of phosphatidylcholine bilayer membranes in the presence of cholesterol, ergosterol and lanosterol: a comparative study using 2h-, ^{13}C- and ^{31}P-NMR spectroscopy, *Biochim. Biophys. Acta, Biomembr.*, 1995, **1238**, 163.
15 T. Thalia, G. Mills, E. Toombes, S. Tristram-Nagle, M. Smilgies, G. Feigenson and J. F. Nagle, Order parameters and areas in fluid-phase oriented lipid membranes using wide angle X-ray scattering, *Biophys. J.*, 2008, **95**, 669.
16 F. de Meyer and B. Smit, Effect of cholesterol on the structure of a phospholipid bilayer, *Proc. Natl. Acad. Sci. U. S. A.*, 2009, **106**, 3654.
17 N. Kucerka, S. Tristram-Nagle and J. F. Nagle, Closer Look at Structure of Fully Hydrated Fluid Phase DPPC Bilayers, *Biophys. J.*, 2006, **90**, L83.
18 O. Berger, O. Edholm and F. Jahnig, Molecular dynamics simulations of a fluid bilayer of dipalmitoylphosphatidylcholine at full hydration, constant pressure, and constant temperature, *Biophys. J.*, 1997, **72**, 2002.
19 D. P. Tieleman, L. R. Forrest, M. Sansom and H. J. C. Berendsen, Lipid Properties and the Orientation of Aromatic Residues in OmpF, Influenza M2, and Alamethicin Systems: Molecular Dynamics Simulations, *Biochemistry*, 1998, **37**, 17554.
20 M. Holtje, T. Forster, B. Brandt, T. Engels, W. von Rybinski and H. D. Holtje, Molecular dynamics simulations of stratum corneum lipid models: fatty acids and cholesterol, *Biochim. Biophys. Acta*, 2001, **1511**, 156.
21 P. Niemela, M. T. Hyvonen and I. Vattulainen, Structure and Dynamics of Sphingomyelin Bilayer: Insight Gained through Systematic Comparison to Phosphatidylcholine, *Biophys. J.*, 2004, **87**, 2976.
22 S. Y. Bhide, Z. Zhang and M. L. Berkowitz, Molecular dynamics simulations of SOPS and sphingomyelin bilayers containing cholesterol, *Biophys. J.*, 2007, **92**, 1284.

23 A. Polley, S. Vemparala and M. Rao, Atomistic simulations of a multicomponent asymmetric lipid bilayer, *J. Phys. Chem. B*, 2012, **116**, 13403.
24 T. Rivel, C. Ramseyer and S. Yesylevskyy, The asymmetry of plasma membranes and their cholesterol content influence the uptake of cisplatin, *Sci. Rep.*, 2019, **9**, 5627.
25 M. Klahn and M. Zacharias, Transformations in plasma membranes of cancerous cells and resulting consequences for cation insertion studied with molecular dynamics, *Phys. Chem. Chem. Phys.*, 2013, **15**, 14427.
26 H. I. Ingolfsson, T. S. Carpenter, H. Bhatia, P.-T. Bremer, S. J. Marrink and F. C. Lightstone, Computational Lipidomics of the Neuronal Plasma Membrane, *Biophys. J.*, 2017, **113**, 2271.
27 W. Helfrich, Elastic properties of lipid bilayers: theory and possible experiments, *Z. Naturforsch.*, 1973, **C28**, 693.
28 P. B. Canham, The minimum energy of bending as a possible explanation of the biconcave shape of the human red blood cell, *J. Theor. Biol.*, 1970, **26**, 61.
29 E. R. May, A. Narang and D. I. Kopelevich, Role of molecular tilt in thermal fluctations of lipid membranes, *Phys. Rev. E: Stat., Nonlinear, Soft Matter Phys.*, 2007, **76**, 021913.
30 R. J. Ryham, T. S. Klotz, L. Yao and F. S. Cohen, Calculating Transition Energy Barriers and Characterizing Activation States for Steps of Fusion, *Biophys. J.*, 2016, **110**, 1110.
31 M. C. Watson, E. S. Penev, P. M. Welch and F. L. H. Brown, Thermal fluctuations in shape, thickness, and molecular orientation in lipid bilayer, *J. Chem. Phys.*, 2011, **135**, 244701.
32 M. C. Watson, E. G. Brandt, P. M. Welch and F. L. H. Brown, Determining biomembrane bending rigidities from simulations of modest size, *Phys. Rev. Lett.*, 2012, **109**, 028102.
33 Z. A. Levine, R. M. Venable, M. C. Watson, M. G. Lerner, J. E. Shea, R. W. Pastor and F. L. H. Brown, Determination of Biomembrane Bending Moduli in Fully Atomistic Simulations, *J. Am. Chem. Soc.*, 2014, **136**, 13582.
34 R. M. Venable, F. L. H. Brown and R. W. Pastor, Mechanical properties of lipid bilayers from molecular dynamics simulation, *Chem. Phys. Lipids*, 2015, **192**, 60.
35 G. Khelashvili, B. Kollmitzer, P. Heftberger, G. Pabst and D. Harries, Calculating the Bending Modulus for Multicomponent Lipid Membranes in Different Thermodynamic Phases, *J. Chem. Theory Comput.*, 2013, **9**, 3866.
36 C. Allolio, A. Haluts and D. Harries, A local instantaneous surface method for extracting membrane elastic moduli from simulation: Comparison with other strategies, *Chem. Phys.*, 2018, **514**, 31.
37 M. Doktorova, D. Harries and G. Khelashvili, Determination of bending rigidity and tilt modulus of lipid membranes from real-space fluctuation analysis of molecular dynamics simulations, *Phys. Chem. Chem. Phys.*, 2017, **19**, 16806.
38 W. Jiang, Y. C. Lin and Y. L. Luo, Mechanical properties of anionic asymmetric bilayers from atomistic simulations, *J. Chem. Phys.*, 2021, **154**, 224701.
39 Y. F. Liu and J. F. Nagel, Diffuse scattering provides material parameters and electron density profiles of biomembranes, *Phys. Rev. E: Stat., Nonlinear, Soft Matter Phys.*, 2004, **69**, 040901.
40 J. F. Nagel, Introductory Lecture: Basic quantities in model biomembranes, *Faraday Discuss.*, 2013, **161**, 11.
41 D. L. Daleke, Regulation of phospholipid asymmetry in the erythrocyte membrane, *Curr. Opin. Hematol.*, 2008, **15**, 191–195.
42 R. F. A. abd, A. J. V. Zwaal, B. Roelofsen, P. Comfurius, D. Kastelijn and L. van Deenen, The asymmetric distribution of phospholipids in the human red cell membrane. A combined study using phospholipases and freeze-etch electron microscopy, *Biochim. Biophys. Acta*, 1973, **323**, 178.
43 A. Zachowski, Phospholipids in animal eukaryotic membranes: transverse asymmetry and movement, *Biochem. J.*, 1993, **294**, 1.
44 G. van Meer, D. R. Voelker and G. W. Feigenson, Membran lipids: where they are and how they behave, *Nat. Rev. Mol. Cell Biol.*, 2008, **9**, 112.
45 A. D. M. Jr, D. Bashford, M. Bellott, R. L. Dunbrack, J. D. Evanseck, M. J. Field, S. Fischer, J. Gao, H. Guo and S. Ha, *et al.*, All-atom empirical potential for molecular modeling and dynamics studies of proteins, *J. Phys. Chem. B*, 1998, **102**, 3586–3616.
46 W. L. Jorgensen, J. Chandrasekhar, J. D. Madura, R. W. Impey and M. L. Klein, Comparison of simple potential functions for simulating liquid water, *J. Chem. Phys.*, 1983, **779**, 926–935.
47 E. Lindahl, B. Hess and D. van der Spoel, GROMACS 3.0: A Package for Molecular Simulation and Trajectory Analysis, *J. Mol. Model.*, 2001, **7**, 306–317.
48 H. J. C. Berendsen, J. P. M. Postma, W. F. van Gunsteren, A. Dinola and J. R. Haak, Molecular-Dynamics With Coupling to an External Bath, *J. Chem. Phys.*, 1984, **81**, 3684–3690.
49 T. Darden, D. York and L. Pedersen, Particle Mesh Ewald: An NÂ·log(N) Method for Ewald Sums in Large Systems, *J. Chem. Phys.*, 1993, **98**, 10089–10092.
50 V. Gapsys, B. L. de Groot and R. Briones, Computational analysis of local membrane properties, *J. Comput.-Aided Mol. Des.*, 2013, **27**, 845.
51 W. Allen, J. Lemkul and D. Bevan, GridMAT-MD: a grid-based membrane analysis tool for use with molecular dynamics, *J. Comput. Chem.*, 2009, **30**, 1952.
52 G. Shahane, W. Ding, M. Palaiokostas and M. Orsi, Physical properties of model biological lipid bilayers: insights from all-atom molecular dynamics simulations, *J. Mol. Model.*, 2019, **25**, 76.
53 T. Asawakarn, J. Cladera and P. O'Shea, Effects of the membrane dipole potential on the interaction of saquinavir with phospholipid membranes and plasma membrane receptors of Caco-2 cells, *J. Bio. Chem.*, 2001, **276**, 38457.
54 L. S. Vermeer, B. L. de Groot, V. Reat, A. Milon and J. Czaplicki, Acyl chain order parameter profiles in phospholipid bilayers: computation from molecular dynamics simulations and comparison with 2H NMR experiments, *Eur. Biophys. J.*, 2007, **36**, 919–931.

55 J. N. Sachs, P. S. Crozier and T. B. Woolf, Atomistic simulations of biologically realistic transmembrane potential gradients, *J. Chem. Phys.*, 2004, **121**, 10847.
56 F. A. Heberle and G. W. Feigenson, Phase Separation in Lipid Membranes, *Cold Spring Harbor Perspect. Biol.*, 2011, **3**, a004630.
57 H. P. Duwe and E. Sackmann, Bending elasticity and thermal excitations of lipid bilayer vesicles: Modulation by solutes, *Phys. A*, 1990, **163**, 410.
58 H. T. McMahon and E. Boucrot, Membrane curvature at a glance, *J. Cell Sci.*, 2015, **128**, 1065.
59 W. Shinoda, Permeability across lipid membranes, *Biochim. Biophys. Acta, Biomembr.*, 2016, **1858**, 2254–2265.
60 J. Chaudhary and M. Munshi, Scanning electron microscopic analysis of breast aspirates, *Cytopathology*, 1995, **6**, 162.
61 I. Dobrzynska, B. Szachowicz-Petelska, S. Sulkowski and Z. Figaszewski, Changes in electric charge and phospholipids composition in human colorectal cancer cells, *Mol. Cell. Biochem.*, 2005, **276**, 113.
62 S. Chakraborty, M. Doktorova, T. R. Molugu, F. A. Heberle, H. L. Scott, B. Dzikovski, M. Nagao, L. R. Stingaciu, R. F. Standaert and F. N. Barrera, *et al.*, How cholesterol stiffens unsaturated lipid membranes, *Proc. Natl. Acad. Sci. U. S. A.*, 2021, **117**, 21896.
63 J. F. Nagle, E. A. Evans, P. Bassereau, T. Baumgart, S. Tristrm-Nagle and R. Dimova, A needless but interesting controversy, *Proc. Natl. Acad. Sci. U. S. A.*, 2021, **118**, e2025011118.
64 R. Ashkar, M. Doktorova, F. A. Heberle, H. L. Scott, F. N. Barrera, J. Katsaras, G. Khelashvili and M. F. Brown, Reply to Nagle et al: The universal stiffening effects of cholesterol on lipid membranes, *Proc. Natl. Acad. Sci. U. S. A.*, 2021, **118**, e2102845118.
65 M. Winterhalter and W. Helfrich, Bending Elasticity of Electrically Charged Bilayers – Coupled Monolayers, Neutral Surfaces, and Balancing Stresses, *J. Phys. Chem.*, 1992, **96**, 327.
66 S. May, Curvature elasticity and thermodynamic stability of electrically charged membranes, *J. Chem. Phys.*, 1996, **105**, 8314.
67 A. Calzado-Martin, M. Encinar, J. Tamayo, M. Calleja and A. S. Paulo, Effect of actin organization on the stiffness of living breast cancer cells revealed by peak-force modulation atomic force microscopy, *ACS Nano*, 2016, **10**, 3365.
68 W. H. Gu, X. Bai, K. L. Ren, X. Y. Zhao, S. B. Xia and J. X. Zhang, *et al.*, Mono-fullerenols modulating cell stiffness by perturbing actin bundling, *Nanoscale*, 2018, **10**, 1750.
69 K. Ren, J. Gao and D. Han, AFM Force Relaxation Curve Reveals That the Decrease of Membrane Tension Is the Essential Reason for the Softening of Cancer Cells, *Front. Cell Dev. Biol.*, 2021, **9**, 663021.
70 M. A. Ayee and I. Levitan, Membrane Stiffening in Osmotic Swelling: Analysis of Membrane Tension and Elastic Modulus, *Curr. Top. Membr.*, 2018, **81**, 97.
71 H. Giang, R. Shlomovitz and M. Schick, Microemulsions, modulated phases and macroscopic phase separation: a unified picture of rafts, *Essays Biochem*, 2015, **57**, 21.
72 R. R. Netz and P. Pincus, Inhomogeneous fluid membranes: Segregation, ordering, and effective rigidity, *Phys. Rev. E: Stat., Nonlinear, Soft Matter Phys.*, 1995, **52**, 4114.
73 S. O. Yesylevskyy, T. Rivel and C. Ramseyer, The influence of curvature on the properties of the plasma membrane. Insights from atomistic molecular dynamics simulations, *Sci. Rep.*, 2017, **7**, 16078.